Detailed small-scale characterization and scale-up of active YFP inclusion body production with *Escherichia coli* induced by a tetrameric coiled coil domain

Short title: Production of Active Inclusion Bodies

Robin Lamm[1,3], Vera D. Jäger[2,3], Benedikt Heyman[1], Christoph Berg[1], Christin Cürten[1,3], Ulrich Krauss[2,3], Karl-Erich Jaeger[2,3,4], Jochen Büchs[1,3]*

[1]AVT - Biochemical Engineering, RWTH Aachen University, D-52074 Aachen, Germany

[2]Institute of Molecular Enzyme Technology, Heinrich Heine University Düsseldorf, Forschungszentrum Jülich GmbH, D-52425 Jülich, Germany

[3]Bioeconomy Science Center (BioSC), D-52425 Jülich, Germany

[4]Institute of Bio- and Geosciences IBG-1: Biotechnology, Forschungszentrum Jülich GmbH, D-52425 Jülich, Germany

*__Correspondence:__ Prof. Dr. Jochen Büchs, AVT - Biochemical Engineering, RWTH Aachen University, Forckenbeckstraße 51, D-52074 Aachen

E-mail: Jochen.buechs@avt.rwth-aachen.de

Phone: +49 (0)241 80 - 24633

Fax: +49 241 80-22570

Keywords: Active inclusion bodies, Fluorescent protein, Online monitoring, Process characterization, High-throughput technologies, Scale-up

Abstract

During heterologous protein production with *E. coli*, the formation of inclusion bodies (IBs) is often a major drawback as these aggregated proteins are usually inactive. However, different strategies for the generation of IBs consisting of catalytically active proteins have recently been described. In this study, the archaeal tetrameric coiled-coil domain of the cell-surface protein tetrabrachion was fused to a target reporter protein to produce fluorescent IBs (FIBs). As the cultivation conditions severely influence IB formation, the entire cultivation process resulting in the production of FIBs were thoroughly studied. First, the cultivation process was scaled down based on the maximum oxygen transfer capacity, combining online monitoring technologies for shake flasks and microtiter plates with offline sampling. The evaluation of culture conditions in complex terrific broth autoinduction medium showed strong oxygen limitation and leaky expression. Furthermore, strong acetate formation and pH changes from 6.5 to 8.8 led to sub-optimal cultivation conditions. However, in minimal Wilms-MOPS autoinduction medium defined culture conditions and a tightly controlled expression was achieved. The production of FIBs is strongly influenced by the induction strength. With increasing induction strength lower total amounts of functional protein but higher amounts of FIBs are obtained. Furthermore, to prevent the formation of conventional inactive IBs, a temperature shift from 37°C to 15°C is crucial to generate FIBs. Finally, the gained insights were transferred to a stirred tank reactor batch fermentation. Hereby, 12 g/L FIBs were produced, making up 43 % (w/w) of the total generated biomass.

Production of Active Inclusion Bodies

Introduction

The application of enzymes in synthetic chemistry is a promising approach due to their high specificities and stereoselectivities that are often not achieved by chemical catalysts (1, 2). Nevertheless, enzymes often lack stability under harsh process conditions like extreme pH, high temperatures, or in non-conventional reaction media that are commonly applied to enable economically feasible processes (3). Immobilization represents a common strategy to increase enzyme stability and recyclability (4-8). However, due to chromatographic purification steps during enzyme isolation and subsequent immobilization protocols, enzyme immobilization is usually laborious and therefore costly (9). Hence, it is highly important to develop generic methods for the simple and cost-efficient production of stable enzyme immobilizates.

Bacterial inclusion bodies (IBs) are protein aggregates that are often formed intracellularly during high-level heterologous protein production (10). These IBs can easily be purified from the culture broth. However, their lack of activity hinders utilization in biocatalysis and synthetic chemistry (11). Recently, it was demonstrated that under certain conditions, IBs can retain catalytic activity (9, 12). Amongst other strategies, the fusion of aggregation-prone tags to enzymes can induce the formation of catalytically active inclusion bodies (CatIBs). Besides CatIBs, fluorescent IBs (FIBs) have often been produced by using a fluorescent reporter protein as a target protein. Garcia-Fruitos et al. (13) fused different aggregation-prone tags to a galactosidase and two fluorescent proteins and obtained active IBs with all fusion proteins. Similarly, Nahalka and Nidetzky (14) showed that the fusion of the cellulose-binding domain of *Clostridium cellulovorans* to a target enzyme leads to formation of CatIBs. In the fusion strategy described by Diener et al. (15), the small (53 amino acids), tetrameric coiled-coil domain of the cell-surface protein tetrabrachion (TDoT) of the deep-sea archaeon *Staphylothermus marinus* is fused to different proteins. Additionally, a short flexible linker peptide is fused between the coiled-coil domain and the target protein. The linker consists of a $(GGGS)_3$ motif and a cleavage site for the protease factor Xa (hereafter referred to as L). Diener et al. (15) showed that at least 80 % of the overall measured activity was found in CatIBs for three enzymes of increasing structural complexity (monomeric lipase A of *Bacillus subtilis*, dimeric *Arabidopsis thaliana* hydroxy nitrile lyase and a dimeric thiamine diphosphate dependent synthase of *E. coli*).

Production of Active Inclusion Bodies

Existing studies comprise the engineering of aggregation-prone tags, computational predictions of polypeptide aggregation and investigations about the morphology and structure of IBs (See reviews by Krauss et al. (9), Rinas et al. (12) and de Marco et al. (16)). In a few studies, the impact of different cultivation parameters on CatIB formation has been investigated (17-22). However, depending on the aggregation-prone tag and the fusion strategy, the impact of cultivation parameters can vary regarding the amount and activity of IBs. Furthermore, most studies focus on one specific cultivation parameter, which hampers the comparability.

To compare active IBs as new immobilized biocatalysts with state-of-the-art biocatalysts, competitive production processes have to be developed for efficient active IB production. However, to enable the development of production processes, knowledge about the impact of different cultivation parameters is crucial, which is currently not available for the fusion strategy described by Diener et al. (15) and others (23-27). Therefore, we have characterized the cultivation process for FIBs production with *E. coli* and investigated the impact of important cultivation parameters (medium composition, oxygen availability, temperature, induction strength) for active IBs production. To enable online monitoring and a higher degree of parallelization, the cultivation protocol published by Diener et al. (15) was scaled down from 5 L shake flasks to 250 mL shake flasks and 48-deepwell microtiter plates (MTPs) (28). Thereby, for the first time, the production of FIBs was in-depth characterized using the Respiration Activity MOnitoring System (RAMOS) (29) and the BioLector technology (30) at defined cultivation conditions. As it has been shown before in multiple studies, data derived from these culture devices can directly be used for scale up to stirred tank reactors (31-33). After investigating the impact of the aforementioned cultivation parameters, FIBs were produced in a 2 L stirred tank reactor batch fermentation at increased carbon concentrations to determine process specific performance indicators like the final FIB titers and space-time-yield.

MATERIALS AND METHODS

Microorganisms and media The gene fusions encoding the fusion protein TDoT-L-YFP and a soluble control construct lacking the TDoT coiled-coil domain (Fig. 1A, C) were produced in *E. coli* BL21(DE3) employing pET28a (Novagen, Darmstadt, Germany) as expression vector (27). The employed variant of the yellow fluorescent protein (YFP) is a monomeric version of enhanced YFP bearing the A206K mutation

(34, 35) but lacking the Q69K mutation, which renders mYFP less pH-sensitive in the neutral pH range (36). During oxygen depended YFP maturation, equimolar H_2O_2 is formed. The toxic effect of H_2O_2 should be taken into account for investigations focusing on redox-related mechanisms as this can influence the measured redox potential (37). As this study focuses on heterologous protein production, the additional H_2O_2 formation can be neglected (38). All cultivation media were supplemented with 0.05 g/L kanamycin for plasmid maintenance. For cultivations in complex media, lysogeny broth (LB) medium was applied as pre-culture (5 g/L yeast extract, 10 g/L tryptone, 10 g/L NaCl) and premixed terrific broth (TB) medium (12 g/L casein, 24 g/L yeast extract, 9.4 g/L K_2HPO_4, 2.2 g/L KH_2PO_4) supplemented with 5 g/L glycerol, 2 g/L lactose and 0.5 g/L glucose was used as main culture (15, 39). Cultivations in minimal media were performed with modified Wilms-MOPS medium (40) according to Rahmen et al. (41) with a pH-value set to 7.5 with NaOH. Pre-cultures in modified Wilms-MOPS medium were supplemented with 5 g/L glucose. Main cultures were supplemented with 5 g/L glycerol, 2 g/L lactose and 0.5 g/L glucose if not stated otherwise. All medium solutions were sterilized separately by autoclaving or filtration before mixing.

Cultivation with online monitoring and offline sampling The pre-cultures in LB medium were inoculated from a cyro culture (OD_{600} 0.02), which was stored at -80 °C and cultivated according to Diener et al. (15) (25 mL filling volume in 250 mL shake flask; 130 rpm, 50 mm shaking diameter, 37 °C cultivation temperature). The main culture in TB autoinduction medium was inoculated with OD_{600} 0.05. Unless stated otherwise, the cultivations were performed in 250 mL shake flasks with 25 mL filling volume at 90 rpm and 50 mm shaking diameter or in 48-deepwell MTPs (m2plabs, Baesweiler, Germany) with 2 mL filling volume at 600 rpm and 3 mm shaking diameter. Pre-cultures in minimal Wilms-MOPS medium were inoculated from a cyro culture (OD_{600} 0.02) and incubated over-night. The pre-cultures were performed in 250 mL shake flasks with 10 mL filling volume at 350 rpm and 50 mm shaking diameter. Unless stated otherwise, the main cultivation in minimal Wilms-MOPS medium was performed in 48-deepwell MTPs (m2plabs, Baesweiler, Germany) with 2 mL filling volume at 600 rpm and 3 mm shaking diameter.

The oxygen transfer rate (OTR) in shake flasks was monitored by applying the Respiration Activity MOnitoring System (RAMOS) built in-house. Commercial versions of the device can be purchased from

Production of Active Inclusion Bodies

Kuhner AG, Switzerland or HiTec Zang GmbH, Germany (29, 42). The oxygen transfer rate (OTR) in 48-deepwell MTPs was monitored by applying the micro Respiration Activity MOnitoring System (µRAMOS) built in-house (43). Online fluorescence ($\lambda_{ex}/\lambda_{em}$ 515/530 nm) and scattered light ($\lambda_{ex}/\lambda_{em}$ 620/620 nm) measurements were performed using in-house built BioLector devices (44, 45). From all displayed online data (fluorescence and scattered light) the initial intensity is subtracted ($I - I_0$). To reduce noise of raw online data from Fig. 2, a median filter with a window size of seven was applied. Similar to the experimental procedure by Wewetzer et al. (46) and Kreyenschulte et al. (47), a data set combining online monitoring and offline sampling during cultivation is derived from multiple individual cultivations in shake flasks and wells of a 48-deepwell microtiter plate. Wells subjected to offline sampling during cultivation are not used for online monitoring. Fig. S1 visualizes the experimental procedure.

Offline analysis For offline sampling, the complete culture broth from single wells was taken out at different time points as indicated. After sampling, the used wells were not subjected to further online analysis.

The formation of inclusion bodies was detected using an inverted Nikon Eclipse Ti microscope (Nicon GmbH, Düsseldorf, Germany) equipped with an Apo TIRF 100X Oil DIC N objective (ALA OBJ-Heater, Ala Scientific Instruments, USA), and ANDOR Zyla CMOS camera (Andor Technology plc., Belfast, UK), an Intensilight (Nicon GmbH, Düsseldorf, Germany) light source for fluorescence excitation, and a fluorescence filter for YFP (excitation 520/60 nm, dichroic mirror: 510 nm, emission: 540/40 nm) (AHF Analysetechnik, Tübingen Germany).

The optical density was determined with a spectrophotometer (Genesys 20, Thermo Fisher Scientific, USA) at a wavelength of 600 nm in 1 cm cuvettes. The sample was appropriately diluted to measure values below 0.4 using 0.9% NaCl (mineral medium) or TB medium (complex medium). NaCl and TB medium were used as blanks.

Production of Active Inclusion Bodies

The pH-value was determined with an InLab Easy pH electrode (Mettler Toledo, Germany) that was calibrated using the appropriate calibration buffers and a CyberScan pH 510 meter (Eutech Instruments, Thermo Scientific, Germany).

In order to quantify the amount of FIBs formed during cultivation, the cells were lysed and the insoluble and soluble cell fractions were separated. Cell lysis was performed in 48-deepwell MTPs. First, the MTP was centrifuged for 3 minutes at 4000 rpm and 4 °C (Hettich Rotina 35R, Germany). The supernatant was discarded. The cell pellets were resuspended in 200 µL of a lysis mastermix (Bugbuster, Merck supplemented with 25 U Benzonase, Merck and 0.2 g/L lysozyme, Carl Roth) and incubated for 15 min at 700 rpm and room temperature. Then, 600 µL lysis buffer (35.6 g/L $Na_2HPO_4 \cdot 2\ H_2O$, 27.6 g/L NaH_2PO_4, 5.8 g/L NaCl) were added to obtain the crude cell extract (CCE). Afterwards, the MTP was centrifuged for 3 minutes at 4000 rpm and 4 °C (Hettich Rotina 35R, Germany). The supernatant (soluble fraction) was carefully transferred into a new 48-deepwell MTP to measure the fraction of soluble YFP. The insoluble pellet (insoluble fraction) was washed with lysis buffer and then used for further analysis (fluorescence measurements, SDS-PAGE). To allow a comparison of the online monitored and offline measured YFP fluorescence, the sample volume was adjusted to retain the same concentration as during cultivation. At high YFP concentration (e.g. at the end of cultivation), inner filter effects are measured (Fig. S2). Therefore, a non-linear relationship between the YFP fluorescence intensity and the amount of YFP may be present. The data in Fig. S2B, which depicts the YFP fluorescence of the soluble fraction of the reference strain (L-YFP) at different concentrations, shows this non-linear relationship. Fig. S2D schematically illustrates the occurring inner filter effect. Since even in diluted samples YFP is highly concentrated inside the inclusion bodies, inner filters effects occur that prevent quantification of the proportion of active to inactive YFP in inclusion bodies (Fig. S2). Therefore, only relative values are given throughout this study (48). Fig. S2C schematically illustrates the occurring inner filter effect for FIBs. Offline YFP fluorescence was measured by a BioLector prototype, which is controlled by a LabVIEW software developed by ZUMOLab, Wesseling Germany.

Sodium dodecylsulfate polyacrylamide gel electrophoresis (SDS-PAGE) was performed to determine the protein distribution in the soluble and insoluble cell fraction. The samples were appropriately diluted with

a defined sample/water ratio and mixed with four-fold concentrated NuPAGE® LDS Sample Buffer (Thermo Fisher Scientific, USA). The prepared samples were placed on a thermo shaker and incubated at 600 rpm and a temperature of 95 °C for 5 min. For protein separation, 17-well or 12-well NuPAGE® 4-12% Bis-Tris gradient gels were used (Thermo Fisher Scientific, USA) and 10 or 20 µL sample were loaded per gel lane, respectively. Electrophoresis was carried out using XCell SureLock™ Mini-Cell electrophoresis system (Invitrogen, Germany) set to 200 V, 0.25 W for 35-45 min. Afterwards, the gels were stained over night at room temperature in Roti®-Blue staining solution (Roth, Germany) and destained using deionized water. The gels were scanned using an Epson perfection V700 photo scanner (Epson, Japan). The distribution of the target protein in the soluble and insoluble fraction was determined by the GelAnalyzer software version 19.1.

The concentration of the different carbon sources and overflow metabolites (glycerol, lactose, glucose and acetate) was determined via ion-exclusion chromatography analysis. An organic acid resin column (250 x 8 mm, CS Chromatographie Services, Germany) was used for separation at a temperature of 80 °C and a flow rate of 0.8 mL/min. As a mobile phase 75 mM H_2SO_4 was used. For the determination of lactose in complex TB medium, anion exchange chromatography according to Anders et al. (49) was performed.

Down scale from 5 L shake flask To enable online monitoring and a higher degree of parallelization a down scale from 5 L shake flask as used by Diener et al. (15) to 250 mL shake flask was performed. Therefore, the maximum oxygen transfer capacity was calculated according to equation (1) from Meier et al. (50)

$$OTR_{max} = 3.72 \cdot 10^{-7} \cdot Osmol^{0.05} \cdot n^{\left(1.18-\frac{Osmol}{10.1}\right)} \cdot {V_L}^{-0.74} \cdot {d_0}^{0.33} \cdot d^{1.88} \cdot p_R \cdot {y_{O_2}}^{*} \qquad (1)$$

For the scale down, the osmolality of the medium (*Osmol*), the absolute pressure (p_R) and the oxygen concentration of the gas phase (y_{O2}^*) were constant for all scales. For the calculation of the maximum oxygen transfer capacity of the 5 L shake flask, the shaking frequency (n = 130 rpm), filling volume (V_L = 500 mL), shaking diameter (d_0 = 50 mm) and the diameter of the flask (d = 216.4 mm) were set to values as described by Diener et al. (15) For the scale down to 250 mL shake flask, the relative filling

volume was kept constant at 10 % and the shaking frequency was calculated to retain the same maximum oxygen transfer capacity as for the 5 L shake flask.

Batch fermentation in stirred tank reactor A Satorius BIOSTAT® Bplus fermenter (Sartorius, Göttingen Germany) with two six-blade Rushton turbines (5.3 cm diameter) were used. The working volume was 1.5 L. For aeration, a ring sparger with 0.5 vvm compressed air was used. The dissolved oxygen tension was controlled at 30 % air saturation by adjusting the stirring rate. The pH was controlled to pH 7 using a 25 % (w/v) ammonia solution. As ammonia was added due to pH control, the initial ammonium concentration was reduced to 10 %. The MOPS buffer was completely omitted from the mineral Wilms-MOPS medium. As the medium osmolality is thereby reduced, an additional amount of initial carbon was added to reach the same osmolality, compared to the cultivation in MTPs with the highest initial carbon concentration (Cx3 medium with 1.5 g/L glucose, 6 g/L lactose and 15 g/L glycerol shown in Fig. S3). Thus, the batch fermentation medium was prepared with 4.9 g/L glucose, 19.7 g/L lactose and 49.2 g/L glycerol. To determine cell dry weight, 1.9 mL culture broth was centrifuged for 3 min at 14,000 rpm (1-15 Sigma Laborzentrifugen, Germany) in dried pre-weighed 2 mL tubes in duplicates. After the supernatant was discarded, cell pellets were dried overnight and weighed. FIBs were isolated as described above and centrifuged in dried pre-weighted tubes. The pelletized FIBs were then dried overnight and weighted to determine the FIB concentration.

RESULTS AND DISCUSSION

The expression of a fusion protein consisting of TDoT-L-YFP leads to the formation of fluorescent inclusion bodies (FIBs) that contain high amounts of functional yellow fluorescent proteins (YFP) (9, 27). The cultivation protocol with terrific broth (TB) auto-induction medium for the production of TDoT-L-YFP FIBs can be divided into two phases. In the first phase, *E. coli* grows on glucose as the preferred carbon source at a cultivation temperature of 37 °C. In the second phase, TDoT-L-YFP expression is induced due to the parallel consumption of lactose and glycerol, and the temperature is reduced to 15 °C (15, 39). The produced FIBs are easily detectable by fluorescence microscopy and via the isolation of insoluble cell components after cell lysis. The YFP constructs, microscopy images of the respective strains

after production of the fusion protein, and the intracellular distribution of YFP fluorescence are shown in Figure 1.

As a reference, a fusion protein consisting only of the linker peptide and YFP but lacking the TDoT coiled-coil domain was expressed under equivalent cultivation conditions to exclusively investigate the impact of the TDoT domain on the protein aggregation (Fig. 1C). The expression of this reference construct (L-YFP) leads to the formation of soluble YFP resulting in equally distributed fluorescence within the cell (Fig. 1D) (27).

Down scale from 5 L shake flask The original cultivation process for the production of catalytically active inclusion bodies (CatIBs) published by Diener et al. (15) was performed in 5 L shake flasks. To characterize the cultivation process, a down-scaling from 5 L to 250 mL shake flasks and to 48-deepwell MTPs was conducted to enable online monitoring and a high degree of parallelization (29, 43, 44). As down scaling criterion, the maximum oxygen transfer capacity was chosen. According to Meier et al. (50), the maximum oxygen transfer capacity in shake flasks can be calculated for known cultivation parameters. The osmolality of the medium is also an important parameter for the calculation of the maximum oxygen transfer capacity due to its strong effect on oxygen solubility and diffusivity in cultivation media (51, 52). At first, the maximum oxygen transfer capacity was calculated using the cultivation parameters reported by Diener et al. (15) for the 5 L shake flask according to equation 1. For the 250 mL shake flask, the relative filling volume was kept constant and the shaking frequency was calculated to retain the same maximum oxygen transfer capacity as for the 5 L shake flask. Since no correlation for MTPs is published that takes the osmolality of the medium into account, the µRAMOS technology was used to determine the downscaled cultivation parameters in MTPs (Fig. S4) (43). In summary, the shaking frequency for the 250 mL shake flask was set to 90 rpm with a filling volume of 25 mL and a shaking diameter of 50 mm. For 48-deepwell MTPs, the cultivation parameters were set to 600 rpm shaking frequency, 2 mL filling volume and 3 mm shaking diameter.

Production of Active Inclusion Bodies

Characterization of the FIB production in complex TB autoinduction medium Based on the downscaled cultivation parameters, the production of FIBs in complex TB autoinduction medium according to Diener et al. (15) was characterized with the RAMOS and BioLector technology (Fig. 2).

In addition to the *E. coli* strain (A-E) harboring the TDoT-L-YFP construct (hereafter referred to as FIB strain), the reference *E. coli* strain (F-J) harboring the L-YFP construct (hereafter referred to as reference strain) is cultured. After 3 hours at a cultivation temperature of 37 °C, a temperature shift to 15 °C is conducted. The oxygen transfer rate (OTR) increases exponentially indicating exponential biomass growth within the first 3 hours (Fig. 2A). During that period, HPLC analysis confirms the typical course of initial carbon sources in autoinduction media. Hence, glucose is consumed as preferred carbon source while lactose and glycerol concentrations remain constant (Fig. 2D). Neither YFP fluorescence (Fig. 2C), nor a protein band in the SDS-PAGE analysis (Fig 2E) is detected after 3 h of cultivation, confirming non-inducing conditions due to catabolite repression. After 3 hours, an OTR plateau (6 mmol/L/h) is reached indicating oxygen limited conditions (Fig. 2A) (29). The subsequent consumption of lactose and glycerol leads to the induction of YFP expression without interfering with the cultivation by the addition of an inducer (Fig. 2C, D, E). While lactose acts as the inducer of the *lac* operon, glycerol serves as an additional carbon and energy source (39, 41). Lactose is depleted much earlier (10 h) than glycerol (19 h) (Fig. 2D). A reference cultivation in complex TB medium without the addition of lactose as inducer shows strong YFP fluorescence, which indicates a leaky expression system (Fig. S5). In contrast, the cultivation in minimal Wilms-MOPS medium without addition of lactose shows no YFP fluorescence indicating a tightly regulated expression system. This difference between complex and minimal media has been reported before but is not fully understood yet (39, 53). Due to the oxygen limitation, inhibiting amounts of acetate (5.6 g/L) are formed after 19 h of cultivation (Fig. 2A, D) (54). Consequently, the pH changes strongly due to the production and subsequent consumption of acetate, the uptake of ammonia and the consumption of complex media components (Fig. 2D) (55-57).

A prominent feature of YFP (and all other GFP variants) is the oxygen dependent maturation accompanied by an equimolar generation of hydrogen peroxide after protein synthesis that is required for fluorescence to be measured (58, 59). While this is commonly recognized as drawback of YFP as a reporter protein since

297 the YFP fluorescence may not directly correlate with YFP synthesis, it can also be used as a tool to identify
298 oxygen limited conditions during cultivation (60, 61). Accordingly, during the oxygen limitation only a
299 small increase of online YFP fluorescence is measured due to the oxygen dependent YFP maturation (Fig.
300 2C). Upon appearance of oxygen unlimited conditions (48 h), the online YFP fluorescence increases
301 abruptly as shown by Ladner et al. (45) and Kunze et al. (62). In comparison, the fluorescence intensity of
302 the different fractions increases earlier indicating YFP maturation during sample preparation (Fig. 2C).
303 Furthermore, the SDS-PAGE analysis confirms that the online fluorescence does not depict the actual YFP
304 synthesis rate (Fig. 2E). Beside the protein band of TDoT-L-YFP, other protein bands appear on the SDS-
305 PAGE analysis of the insoluble fraction (Fig. 2E). As described by Kloß et al. (25), active IBs can contain
306 membrane proteins with a size of around 40 kDa (OmpA, OmpF) and chaperones with a size of 15 kDa
307 (IbpA, IbpB). The SDS-PAGE analysis of the insoluble fraction of the FIB strain also reveals protein bands
308 with this protein size (Fig. 2E). Additionally, the SDS-PAGE analysis shows that more than 90% of TDoT-
309 L-YFP (33 kDa) is present within the insoluble fraction indicating the effective formation of inclusion
310 bodies induced by the TDoT domain. This is in agreement with other studies showing the production of
311 active IBs utilizing this tetrameric coiled-coil domain (23, 25). However, the high YFP fluorescence in the
312 soluble fraction shows that TDoT-L-YFP is partly also present in a soluble form. Remarkably, the measured
313 fluorescence intensity is equally high in the soluble and insoluble fraction over the course of the cultivation.
314 This effect might be attributed to the dense packing of YFP within FIBs that leads to lower fluorescence
315 intensities and to an underestimation of active protein due to optical inner filter effects (48). The inner filter
316 effect is schematically illustrated in Fig. S2C.
317
318 In contrast to the FIB strain (containing TDoT-L-YFP), the reference strain (containing L-YFP) shows no
319 formation of FIBs indicated by the absence of fluorescence of the insoluble fraction (Fig. 2H) and the
320 absence of a protein band (27.2 kDa) in the SDS-PAGE analysis in the insoluble fraction (Fig. 2J). As
321 described in the materials and methods, an inner filter effect can also occur at high soluble YFP
322 concentration (Fig. S2B+D). This filter effect is visible when comparing the amount of soluble YFP in the
323 SDS-PAGE analysis (Fig. 2E+J) and the fluorescence intensity of the soluble fraction of the same sample
324 (Fig. 2C+H). The absence of FIBs is also indicated by much lower scattered light intensities of the reference
325 strain compared to the FIB strain (Fig. 2B, G). Similar as conventional inactive IBs, FIBs also scatter light,

and therefore, lead to increased scattered light intensities (63). SDS-PAGE analysis of the cell lysate obtained from the reference strain (Fig. 2H) revealed two bands with a size of approximately 27 kDa and 26 kDa, respectively. This phenomenon was not further investigated but could originate from the cleavage of the linker (1 kDa) from soluble YFP. In the OTR, a strong decrease (24 h) is visible when glycerol and lactose are depleted. The metabolic switch to acetate as carbon source leads to a lower level of oxygen consumption (Fig. 2F, I). This is also visible in the scattered light and OD, which remain constant during that period (20 – 32 h) (Fig. 2G). At the end of oxygen limited conditions (24 h), the YFP online fluorescence intensity increases strongly due to oxygen dependent YFP maturation (Fig. 2F, H, J). The offline YFP fluorescence intensity increases earlier due to YFP maturation during sample preparation (Fig. 2H).

Despite strong oxygen limitation, high acetate formation and strong pH changes, high amounts of FIBs were produced by the FIB strain. However, these sub-optimal cultivation conditions and the leaky expression can be prevented by applying defined minimal media with increased buffer capacities. Furthermore, the carbon flux could be redirected from overflow metabolite formation to FIB production by increasing the maximum oxygen transfer capacity.

Characterization of the FIB production on minimal Wilms-MOPS autoinduction medium To investigate the impact of different cultivation parameters on FIB production, the complex TB medium was replaced by the minimal Wilms-MOPS medium. Thereby, the chemical medium composition is defined, and expression is more controlled (Fig. 3) (41, 53, 64). Also, high batch-to-batch variations that are observed for complex substrates even if they are purchased from the same supplier are avoided (56, 65). Due to the omission of these considerable amounts of complex substrates (12 g/L casein, 24 g/L yeast extract) in minimal Wilms-MOPS autoinduction medium, lower FIB production is expected.

Fig. 3 shows the cultivation of the FIB strain and the reference strain on minimal Wilms-MOPS autoinduction medium. Again, in the first 3 h, an exponential growth on glucose occurs while lactose and glycerol concentrations remain constant (Fig. 3A, C). After 3 h, the temperature shift from 37 °C to 15 °C is conducted. From 3 – 20.5 h, lactose and glycerol are consumed in parallel and YFP expression is induced

(Fig. 3C, D). As shown in Fig. 2, YFP fluorescence increases very slowly during oxygen limiting conditions. Upon depletion of all initial carbon sources (20.5 h), oxygen dependent YFP maturation takes place (Fig. 3B, C). At that time, only small amounts of acetate (0.5 g/L) have been formed compared to the cultivation in complex medium (Fig. 3C). The production of FIBs is confirmed by YFP fluorescence within the insoluble fraction (Fig. 3B). Furthermore, the TDoT-L-YFP protein band (33 kDa) is mainly visible in the insoluble cell fraction (Fig. 3D). Remarkably, the YFP fluorescence distribution between the soluble and insoluble fractions remains constant after depletion of all carbon sources (32.5 – 59 h), even though the scattered light intensity increases (Fig. 3A, B). For the reference strain (L-YFP), no fluorescence is visible within the insoluble cell fraction (Fig. 3F). Additionally, no protein bands are detectable within the insoluble fraction by SDS-PAGE confirming the absence of IBs (Fig. 3H). The pH remains within a narrow range (7.1 – 7.2) over the course of cultivation for both strains (Fig. 3C, G).

As expected, lower amounts of FIBs are produced in minimal Wilms-MOPS autoinduction medium compared to the cultivation in TB autoinduction medium. This is also visible in the scattered light, which is only slightly higher for the FIB strain compared to the reference strain. This deviation is caused by the omission of large amounts of complex substrates (36 g/L complex substrates) compared to 7.5 g/L of sugars (Fig. 2C, 3B). These complex substrates (12 g/L casein, 24 g/L yeast extract) contain a mixture of carbohydrates, amino acids, peptides and trace elements (64). The omission of these complex substrates leads to a lower overall carbon content, which decreases the amounts of produced FIBs. Additionally, the expression in TB autoinduction medium is amplified by leaky expression (Fig. S5). By increasing the amount of glucose, lactose and glycerol, the amount of FIBs can easily be increased in minimal Wilms-MOPS autoinduction medium (Fig. S3).

Cultivation at constant temperature The strong effect of cultivation temperature on conventional IB formation has extensively been studied (66, 67). To prevent IB formation, the cultivation temperature is often lowered to facilitate protein folding and to prevent protein aggregation. In case of FIB production, correct protein folding and protein aggregation is intended at the same time. Therefore, the impact of the temperature shift introduced by Diener et al. (15) was investigated in comparison to cultivations of the FIB strain and the reference strain at a constant cultivation temperature of 37 °C (Fig. 4).

Production of Active Inclusion Bodies

Additional to the standard filling volume of 2 mL, lower filling volumes (1.5, 1.0, 0.6, 0.4 mL) were cultured to obtain increasing maximum oxygen transfer capacities. Within the first 3 h, the oxygen transfer rate of the FIB and the reference strain increases (Fig. 4A, C), while no YFP fluorescence intensity is detectable (Fig. 4A, C). Subsequently, the OTR drops shortly, which indicates the depletion of glucose (41). Afterwards, the OTR increases while lactose and glycerol are consumed, indicated by the increasing YFP fluorescence intensity after 5 hours of cultivation of the reference strain (Fig. 4A, B, C). For lower filling volumes, higher OTRs are reached due to higher oxygen availabilities (Fig. 4A, C). At high filling volumes (2.0, 1.5 and 1.0 mL), OTR plateaus at different levels are reached indicating oxygen limiting conditions. For the reference strain and filling volumes of 1, 1.5 and 2 mL, YFP fluorescence increases abruptly upon oxygen unlimited conditions (16 h, 19 h, 24 h), which is indicated by the OTR drop at the of the OTR plateau. Cultures with 0.4 mL filling volume are not oxygen limited indicated by the absence of an OTR plateau and by the consistently increasing YFP fluorescence (Fig. 4C, D). Except for the cultures with high maximum oxygen transfer capacities (0.4 and 0.6 mL filling volume), lower maximum oxygen transfer capacities lead to lower final fluorescence intensities (Fig. 4C, D). While the reference strain shows high YFP fluorescence intensities, no fluorescence intensity is measured for the FIB strain (Fig. 4B). The SDS-PAGE analysis for the standard filling volume of 2 mL shows mainly soluble YFP for the reference strain and mainly insoluble YFP for the FIB strain at the end of cultivation. Furthermore, the SDS-PAGE analysis shows a similar YFP amount for both strains. For the FIB strain, this indicates the formation of conventional IBs containing misfolded, aggregated, non-fluorescent YFP. Most likely, the protein folding of the entire monomeric fusion protein (TDoT-L-YFP) has first to be completed to be then incorporated in IBs in an active form. It has often been reported that lower cultivation temperatures lead to IBs with higher activity (18-21, 68). However, in other studies, fusion proteins with aggregation-prone tags are produced that lead to the formation of active inclusion bodies even though the expression temperature is not lowered (13, 69-71). Presumably, a higher aggregation tendency of the fusion tag and culture conditions that lead to high local protein concentrations require lower cultivation temperatures to obtain high amounts of actively folded proteins in IBs. In an upcoming publication, the impact of the cultivation temperature is studied in-depth using a MTP-based temperature profiling system established by Kunze et al. (72).

Production of Active Inclusion Bodies

Cultivation with varying maximum oxygen transfer capacities After the necessity of the temperature shift was confirmed, a cultivation with the standard temperature shift at different maximum oxygen transfer capacities was conducted to investigate the effect of oxygen limitation on the FIB production (Fig. 5).

The FIB strain is cultured in minimal Wilms-MOPS autoinduction medium with varying filling volumes (2.0, 1.6, 1.2, 0.6 mL). During the cultivation, a temperature shift after 3 h from 37 °C to 15 °C was conducted as previously described (Fig. 2, 3). Within the first 3 h of cultivation, the scattered light increases exponentially while no YFP fluorescence intensity is detected (Fig. 5A, B). Subsequently, the typical YFP fluorescence course is measured for the standard filling volume (2 mL). A slow linear increase is followed by an abrupt increase upon oxygen unlimited conditions (Fig. 5B) (45, 60, 61). For lower filling volumes, this abrupt increase becomes less prominent due to higher maximum oxygen transfer capacities. At a filling volume of 0.6 mL no oxygen limitation occurs and the YFP fluorescence increases with a steady slope, depicting the actual production rate of TDoT-L-YFP. Eventually, the final YFP fluorescence intensities are similar for different filling volumes (Fig. 5B). Fig. 5C shows the final fluorescence intensities at the end of cultivation of the different fractions. In Fig. S6, the results depicted in Fig. 5C were reproduced and show the same fluorescence distribution between the fractions for different filling volumes. Slightly higher YFP fluorescence intensities are measured in the soluble than in the insoluble fraction as already shown in Fig. 3 (Fig. 5C). It is also obvious that the maximum oxygen transfer capacity has no impact on the final fluorescence intensity of FIBs. However, oxygen limiting conditions lead to several disadvantages like prolonged cultivation times and acidification of the culture broth due to acetate formation. Hence, oxygen limitation has to be avoided.

Impact of induction method and strength on FIB production The induction method and strength is an important cultivation parameter for the production of heterologous proteins as well as active IBs (16, 73). Besides lactose, isopropyl β-D-1-thiogalactopyranoside (IPTG) at different concentrations is used to investigate the impact of induction strength on FIB production (Fig. 6, Fig. S7).

Production of Active Inclusion Bodies

As the cultivation temperature is a crucial cultivation parameter to produce FIBs (Fig. 4), IPTG was added in different concentrations at the same time (after 4.5 h) to induce all cultures at the same temperature (Fig. 6B, black arrow). Within the first 4.5 h of cultivation, scattered light increases similarly for all cultivations. Subsequently, the slopes of scattered light curves are lower at increasing IPTG concentrations (Fig. 6A). For autoinduced cultures, scattered light increases similarly as in cultures with IPTG concentrations of 0.1-0.15 mM. Online YFP fluorescence increases after 4.5 h for all induced cultures (Fig. 6B). The final YFP fluorescence of autoinduced cultures is equal to cultures induced with 0.1 mM IPTG. The highest final YFP fluorescence is measured for cultures induced with 0.05 mM IPTG (Fig. 6B, C). For autoinduced cultures and cultures induced with IPTG concentrations of 0.15-1 mM, the final YFP fluorescence intensities of the crude cell extract and the insoluble fraction are similar. However, lower induction strengths (0.05 and 0.1 mM IPTG) lead to higher YFP fluorescence in the crude cell extract and soluble fraction, while lower YFP fluorescence in the insoluble fraction are measured (Fig. 6C, Fig. S7C). Thus, lower induction strengths shift the amount of YFP from FIBs to the soluble fraction (Fig. S7C). This was already observed in studies dealing with conventional, inactive IBs (22, 74). Higher induction strengths lead to higher expression rates that reduce the production of native soluble protein, but increase the amount of active proteins in IBs (22). Possibly, high local protein concentrations and misfolded proteins function as aggregation nucleus that capture additional native proteins. Thereby, the production of active IBs is increased even though the total amount (soluble and insoluble YFP) of active proteins is reduced. To produce active IBs, it is crucial to find the right balance between a high portion of active proteins and a high amount of proteins aggregated in IBs.

Batch fermentation in stirred tank reactor for the production of FIBs To determine process specific performance indicators like the final FIB titer and space-time-yield and to obtain larger sample volumes, a 2 L batch fermentation with increased amount of carbon sources was performed (Fig. 7). The scalability of the obtained insights on FIB production from the MTP-scale is proven.

As the importance of the temperature shift was demonstrated above, the temperature was reduced from 37 to 15 °C during cultivation (Fig. 7A). At 37 °C exponential growth on glucose takes place and no production of FIBs is observed (Fig. 7A, C, D). Due to the temperature shift and the depletion of glucose, the OTR

drops after around 8 h of cultivation. Subsequently, the OTR increases until the end of fermentation up to 40 mmol/L/h, which is reflected in increasing glycerol and lactose consumption rates (Fig. 7A, D). Interestingly, the hydrolysis of lactose to galactose and glucose leads to the accumulation of up to 4 g/L glucose. Usually, glucose intracellularly produced by lactose hydrolysis is phosphorylated and not secreted into the culture broth (75). Potentially, the low cultivation temperature decelerated glucose phosphorylation, and thus, leads to glucose accumulation. The production of FIBs is confirmed by high YFP fluorescence in the insoluble fraction, which is approximately 10-fold increased compared to the standard cultivation in Wilms-MOPS medium (compare Fig. 7C and Fig. 3B). The production of IBs can also be indirectly inferred from the cell dry weight and optical density curves (Fig. 7B). During initial growth on glucose, the cell dry weight and optical density are similarly increasing. Subsequently, the optical density is increasing much stronger, compared to the cell dry weight, probably due to increased light scattering by the produced FIBs (Fig. 7B). After 53 h of cultivation, the final cell dry weight is 27.6 g/L and the FIB concentration is 11.9 g/L ± 0.15 g/L (Fig. 7E). Thus, a remarkably high biomass-specific FIB yield of 0.43 is achieved (Fig. 7F). The FIB yield per supplemented carbon source is 0.16. Overall, a space-time-yield of 0.23 g/L/h FIBs is reached (Fig. 7F).

To facilitate online monitoring and a higher degree of parallelization, a published cultivation protocol for the production of active IBs was scaled-down, based on the maximum oxygen transfer capacity. Subsequently, the production of fluorescent inclusion bodies (FIBs) in complex TB autoinduction medium was characterized and the impact of important cultivation parameters (cultivation medium, oxygen availability, cultivation temperature, and induction strength) on FIB production was systematically evaluated. The characterization of previously published cultivation protocol for FIB production in complex TB autoinduction medium showed strong oxygen limitation, high acetate formation, strong pH changes and leaky expression. By applying the defined mineral Wilms-MOPS autoinduction medium, tightly controlled expression was achieved, and strong acetate formation and pH shifts were avoided. It was shown that oxygen limiting conditions are not necessary and beneficial to produce FIBs. However, in order to prevent the production of conventional, inactive IBs, the temperature shift from 37 to 15 °C is crucial. Furthermore, a strong impact of the induction strength on FIB production was observed. Low induction strength lead to more active YFP, but lower amounts of active YFP in FIBs. For FIB production, it is therefore vital to find

the right balance between a high induction strength to effectively induce protein aggregation and a higher folding efficiency at lower induction strengths. These observations motivate further investigations regarding the structural differences between conventional inactive IBs and active IBs, as both kinds of IBs can be produced with the same target protein by simply altering the cultivation conditions. Finally, the general applicability and scalability of the gained insights were confirmed in a 2 L stirred tank reactor batch fermentation. Due to the increased amount of supplemented carbon sources, 11.9 g/L of highly active FIBs were produced that made up 43 % (w/w) of the total cell dry weight. Generally, different studies have been published that examine the impact of cultivation conditions on active IB production. However, this study focuses on the systematic investigation of various important cultivation parameters on active IB formation with comprehensive offline and online analyses. Additionally, the scale-up of the results from µL-scale to lab-scale stirred tank reactors was proven. This presented methodology can be extended to other fusion strategies to systematically investigate and compare different fusion strategies for active IB production. In future, the insights on the production of FIBs have to be transferred to catalytically active inclusion bodies (CatIBs).

Acknowledgements

This study was funded by the Bioeconomy Science Center (BioSC), which is financially supported by the Ministry of Culture and Science of North-Rhine Westphalia within the framework of the NRW Strategieprojekt BioSC (Grant No. 313/32 3-400-002 13). BioSC is a research cluster consisting of the universities RWTH Aachen, Düsseldorf and Bonn, and the Forschungszentrum Jülich.

Conflict of interest

The authors declare that they have no conflict of interest.

References

1. **Patel, R., Hanson, R., Goswami, A., Nanduri, V., Banerjee, A., Donovan, M. J., Goldberg, S., Johnston, R., Brzozowski, D., Tully, T., and other X authors:** Enzymatic synthesis of chiral intermediates for pharmaceuticals, J. Ind. Microbiol. Biotechnol., **30**, 252-259 (2003).

2. **Nestl, B. M., Nebel, B. A., and Hauer, B.:** Recent progress in industrial biocatalysis, Curr. Opin. Chem. Biol., **15**, 187-193 (2011).
3. **Castro, G. R. and Knubovets, T.:** Homogeneous biocatalysis in organic solvents and water-organic mixtures, Crit. Rev. Biotechnol., **23**, 195-231 (2003).
4. **Balcao, V. M. and Vila, M.:** Structural and functional stabilization of protein entities: state-of-the-art, Adv. Drug Deliv. Rev., **93**, 25-41 (2015).
5. **Liese, A. and Hilterhaus, L.:** Evaluation of immobilized enzymes for industrial applications, Chem. Soc. Rev., **42**, 6236-6249 (2013).
6. **Guisan, J. M.:** New opportunities for immobilization of enzymes, pp. 1-13, in: Guisan, J. M. (Ed.), Immobilization of Enzymes and Cells, vol.1051. Humana Press Inc, Totowa, NJ, USA (2013).
7. **Sheldon, R. A.:** Characteristic features and biotechnological applications of cross-linked enzyme aggregates (CLEAs), Appl. Microbiol. Biotechnol., **92**, 467-477 (2011).
8. **Tielmann, P., Kierkels, H., Zonta, A., Ilie, A., and Reetz, M. T.:** Increasing the activity and enantioselectivity of lipases by sol-gel immobilization: further advancements of practical interest, Nanoscale, **6**, 6220-6228 (2014).
9. **Krauss, U., Jäger, V. D., Diener, M., Pohl, M., and Jaeger, K. E.:** Catalytically-active inclusion bodies-carrier-free protein immobilizates for application in biotechnology and biomedicine, J. Biotechnol., **258**, 136-147 (2017).
10. **Georgiou, G. and Valax, P.:** Expression of correctly folded proteins in *Escherichia coli*, Curr. Opin. Biotechnol., **7**, 190-197 (1996).
11. **Villaverde, A. and Carrio, M. M.:** Protein aggregation in recombinant bacteria: biological role of inclusion bodies, Biotechnol. Lett **25**, 1385-1395 (2003).
12. **Rinas, U., Garcia-Fruitos, E., Corchero, J. L., Vazquez, E., Seras-Franzoso, J., and Villaverde, A.:** Bacterial Inclusion Bodies: Discovering Their Better Half, Trends Biochem. Sci **42**, 726-737 (2017).
13. **Garcia-Fruitos, E., Gonzalez-Montalban, N., Morell, M., Vera, A., Ferraz, R. M., Aris, A., Ventura, S., and Villaverde, A.:** Aggregation as bacterial inclusion bodies does not imply inactivation of enzymes and fluorescent proteins, Microb. Cell Fact., **4**, 27 (2005).

14. **Nahalka, J. and Nidetzky, B.:** Fusion to a pull-down domain: a novel approach of producing *Trigonopsis variabilis* D-amino acid oxidase as insoluble enzyme aggregates, Biotechnol. Bioeng., **97**, 454-461 (2007).
15. **Diener, M., Kopka, B., Pohl, M., Jaeger, K.-E., and Krauss, U.:** Fusion of a coiled-coil domain facilitates the high-level production of catalytically active enzyme inclusion bodies, ChemCatChem, **8**, 142-152 (2016).
16. **de Marco, A., Ferrer-Miralles, N., Garcia-Fruitos, E., Mitraki, A., Peternel, S., Rinas, U., Trujillo-Roldan, M. A., Valdez-Cruz, N. A., Vazquez, E., and Villaverde, A.:** Bacterial inclusion bodies are industrially exploitable amyloids, FEMS Microbiol Rev, **43**, 53-72 (2019).
17. **Arié, J.-P., Miot, M., Sassoon, N., and Betton, J.-M.:** Formation of active inclusion bodies in the periplasm ofEscherichia coli, Molecular Microbiology, **62**, 427-437 (2006).
18. **de Groot, N. S. and Ventura, S.:** Effect of temperature on protein quality in bacterial inclusion bodies, FEBS Lett., **580**, 6471-6476 (2006).
19. **Doglia, S. M., Ami, D., Natalello, A., Gatti-Lafranconi, P., and Lotti, M.:** Fourier transform infrared spectroscopy analysis of the conformational quality of recombinant proteins within inclusion bodies, Biotechnol. J., **3**, 193-201 (2008).
20. **Vera, A., Gonzalez-Montalban, N., Aris, A., and Villaverde, A.:** The conformational quality of insoluble recombinant proteins is enhanced at low growth temperatures, Biotech. Bioeng. , **96**, 1101-1106 (2007).
21. **Wang, W., Sun, J., Xiao, W., Jiang, L., Wang, R., and Fan, J.:** Change of the N-terminal codon bias combined with tRNA supplementation outperforms the selected fusion tags for production of human D-amino acid oxidase as active inclusion bodies, Biotechnol. Lett, **39**, 1733-1740 (2017).
22. **Jhamb, K. and Sahoo, D. K.:** Production of soluble recombinant proteins in *Escherichia coli*: effects of process conditions and chaperone co-expression on cell growth and production of xylanase, Bioresour Technol, **123**, 135-143 (2012).

23. **Jäger, V. D., Kloss, R., Grünberger, A., Seide, S., Hahn, D., Karmainski, T., Piqueray, M., Embruch, J., Longerich, S., Mackfeld, U., and other X authors:** Tailoring the properties of (catalytically)-active inclusion bodies, Microbial Cell Factories, **18**, 33 (2019).
24. **Jäger, V. D., Piqueray, M., Seide, S., Pohl, M., Wiechert, W., Jaeger, K.-E., and Krauss, U.:** An Enzymatic 2‐Step Cofactor and Co‐Product Recycling Cascade towards a Chiral 1,2‐Diol. Part II: Catalytically Active Inclusion Bodies, Adv Synth Catal (2019).
25. **Kloß, R., Karmainski, T., Jäger, V. D., Hahn, D., Grünberger, A., Baumgart, M., Krauss, U., Jaeger, K. E., Wiechert, W., and Pohl, M.:** Tailor-made catalytically active inclusion bodies for different applications in biocatalysis, Catal. Sci. Technol., **8**, 5816-5826 (2018).
26. **Kloß, R., Limberg, M. H., Mackfeld, U., Hahn, D., Grünberger, A., Jäger, V. D., Krauss, U., Oldiges, M., and Pohl, M.:** Catalytically active inclusion bodies of L-lysine decarboxylase from *E. coli* for 1,5-diaminopentane production, Sci. Rep., **8**, 11 (2018).
27. **Jäger, V. D., Lamm, R., Kloß, R., Kaganovitch, E., Grünberger, A., Pohl, M., Büchs, J., Jaeger, K. E., and Krauss, U.:** A synthetic reaction cascade implemented by colocalization of two proteins within catalytically active inclusion bodies, ACS Synth Biol, **7**, 2282-2295 (2018).
28. **Lattermann, C. and Büchs, J.:** Microscale and miniscale fermentation and screening, Curr. Opin. Biotechnol., **35**, 1-6 (2015).
29. **Anderlei, T. and Büchs, J.:** Device for sterile online measurement of the oxygen transfer rate in shaking flasks, Biochem. Eng. J., **7**, 157-162 (2001).
30. **Samorski, M., Muller-Newen, G., and Büchs, J.:** Quasi-continuous combined scattered light and fluorescence measurements: A novel measurement technique for shaken microtiter plates, Biotech. Bioeng. , **92**, 61-68 (2005).
31. **Kensy, F., Engelbrecht, C., and Büchs, J.:** Scale-up from microtiter plate to laboratory fermenter: evaluation by online monitoring techniques of growth and protein expression in *Escherichia coli* and *Hansenula polymorpha* fermentations, Microb. Cell Fact., **8** (2009).
32. **Seletzky, J. M., Noak, U., Fricke, J., Welk, E., Eberhard, W., Knocke, C., and Büchs, J.:** Scale-up from shake flasks to fermenters in batch and continuous mode with *Corynebacterium*

glutamicum in lactic acid based on oxygen transfer and pH, Biotech. Bioeng., **98**, 800-811 (2007).

33. **Funke, M., Buchenauer, A., Mokwa, W., Kluge, S., Hein, L., Muller, C., Kensy, F., and Büchs, J.:** Bioprocess control in microscale: scalable fermentations in disposable and user-friendly microfluidic systems, Microb. Cell Fact., **9**, 13 (2010).

34. **Zacharias, D. A., Violin, J. D., Newton, A. C., and Tsien, R. Y.:** Partitioning of lipid-modified monomeric GFPs into membrane microdomains of live cells, Science, **296**, 913-916 (2002).

35. **Wachter, R. M., Elsliger, M. A., Kallio, K., Hanson, G. T., and Remington, S. J.:** Structural basis of spectral shifts in the yellow-emission variants of green fluorescent protein, Structure, **6**, 1267-1277 (1998).

36. **Miyawaki, A., Griesbeck, O., Heim, R., and Tsien, R. Y.:** Dynamic and quantitative Ca^{2+} measurements using improved cameleons, Proc. Nat. Acad. Sci. U.S.A. , **96**, 2135-2140 (1999).

37. **Ganini, D., Leinisch, F., Kumar, A., Jiang, J. J., Tokar, E. J., Malone, C. C., Petrovich, R. M., and Mason, R. P.:** Fluorescent proteins such as eGFP lead to catalytic oxidative stress in cells, Redox Biol., **12**, 462-468 (2017).

38. **Kalyanaraman, B. and Zielonka, J.:** Green fluorescent proteins induce oxidative stress in cells: A worrisome new wrinkle in the application of the GFP reporter system to biological systems, Redox Biol., **12**, 755-757 (2017).

39. **Studier, F. W.:** Protein production by auto-induction in high-density shaking cultures, Protein Expr. Purif., **41**, 207-234 (2005).

40. **Wilms, B., Hauck, A., Reuss, M., Syldatk, C., Mattes, R., Siemann, M., and Altenbuchner, J.:** High-cell-density fermentation for production of L-*N*-Carbamoylase using an expression system based on the *Escherichia coli rhaBAD p*romoter, Biotechnol. Bioeng., **73**, 95-103 (2001).

41. **Rahmen, N., Fulton, A., Ihling, N., Magni, M., Jaeger, K. E., and Büchs, J.:** Exchange of single amino acids at different positions of a recombinant protein affects metabolic burden in *Escherichia coli*, Microb. Cell Fact., **14**, 10 (2015).

42. **Anderlei, T., Zang, W., Papaspyrou, M., and Büchs, J.:** Online respiration activity measurement (OTR, CTR, RQ) in shake flasks, Biochem. Eng. J., **17**, 187-194 (2004).

43. **Flitsch, D., Krabbe, S., Ladner, T., Beckers, M., Schilling, J., Mahr, S., Conrath, U., Schomburg, W. K., and Büchs, J.:** Respiration activity monitoring system for any individual well of a 48-well microtiter plate, J. Biol. Eng., **10**, 14 (2016).

44. **Ladner, T., Beckers, M., Hitzmann, B., and Büchs, J.:** Parallel online multi-wavelength (2D) fluorescence spectroscopy in each well of a continuously shaken microtiter plate, Biotechnol. J., **11**, 1605-1616 (2016).

45. **Ladner, T., Held, M., Flitsch, D., Beckers, M., and Büchs, J.:** Quasi-continuous parallel online scattered light, fluorescence and dissolved oxygen tension measurement combined with monitoring of the oxygen transfer rate in each well of a shaken microtiter plate, Microb. Cell Fact., **15** (2016).

46. **Wewetzer, S. J., Kunze, M., Ladner, T., Luchterhand, B., Roth, S., Rahmen, N., Kloß, R., Costa, E. S. A., Regestein, L., and Büchs, J.:** Parallel use of shake flask and microtiter plate online measuring devices (RAMOS and BioLector) reduces the number of experiments in laboratory-scale stirred tank bioreactors, J Biol Eng, **9**, 9 (2015).

47. **Kreyenschulte, D., Heyman, B., Eggert, A., Massmann, T., Kalvelage, C., Kossack, R., Regestein, L., Jupke, A., and Büchs, J.:** In situ reactive extraction of itaconic acid during fermentation of *Aspergillus terreus*, Biochemical Engineering Journal, **135**, 133-141 (2018).

48. **Parker, C. A. and Rees, W. T.:** Fluorescence spectrometry - a review, Analyst, **87**, 83-& (1962).

49. **Anders, N., Humann, H., Langhans, B., and Spiess, A. C.:** Simultaneous determination of acid-soluble biomass-derived compounds using high performance anion exchange chromatography coupled with pulsed amperometric detection, Anal. Methods, **7**, 7866-7873 (2015).

50. **Meier, K., Klöckner, W., Bonhage, B., Antonov, E., Regestein, L., and Büchs, J.:** Correlation for the maximum oxygen transfer capacity in shake flasks for a wide range of operating conditions and for different culture media, Biochem. Eng. J., **109**, 228-235 (2016).

667 51. **Schumpe, A.:** The estimation of gas solubilities in salt-solutions, Chem. Eng. Sci., **48**, 153-
668 158 (1993).
669 52. **Popovic, M., Niebelschutz, H., and Reuss, M.:** Oxygen solubilities in fermentation fluids,
670 Eur. J. Appl. Microbiol. Biotechnol. , **8**, 1-15 (1979).
671 53. **Grossman, T. H., Kawasaki, E. S., Punreddy, S. R., and Osburne, M. S.:** Spontaneous cAMP-
672 dependent derepression of gene expression in stationary phase plays a role in recombinant
673 expression instability, Gene, **209**, 95-103 (1998).
674 54. **Luli, G. W. and Strohl, W. R.:** Compaorison of growth, actetate production, and acetate
675 inhibition of *Escherichia coli* strains in batch and fed-batch fermentations, Appl. Environ.
676 Microbiol., **56**, 1004-1011 (1990).
677 55. **Losen, M., Frölich, B., Pohl, M., and Büchs, J.:** Effect of oxygen limitation and medium
678 composition on *Escherichia coli* fermentation in shake-flask cultures, Biotechnol. Prog., **20**,
679 1062-1068 (2004).
680 56. **Diederichs, S., Korona, A., Staaden, A., Kroutil, W., Honda, K., Ohtake, H., and Büchs, J.:**
681 Phenotyping the quality of complex medium components by simple online-monitored shake
682 flask experiments, Microb. Cell Fact., **13**, 149 (2014).
683 57. **Christensen, M. L. and Eriksen, N. T.:** Growth and proton exchange in recombinant
684 *Escherichia coli* BL21, Enzyme Microb. Technol., **31**, 566-574 (2002).
685 58. **Cody, C. W., Prasher, D. C., Westler, W. M., Prendergast, F. G., and Ward, W. W.:** Chemical-
686 structure of the hexapeptide chromophore of the aequorea green-fluorescent protein,
687 Biochemistry, **32**, 1212-1218 (1993).
688 59. **Zhang, L., Patel, H. N., Lappe, J. W., and Wachter, R. M.:** Reaction progress of chromophore
689 biogenesis in green fluorescent protein, J. Am. Chem. Soc., **128**, 4766-4772 (2006).
690 60. **Drepper, T., Eggert, T., Circolone, F., Heck, A., Krauss, U., Guterl, J. K., Wendorff, M., Losi,**
691 **A., Gartner, W., and Jaeger, K. E.:** Reporter proteins for in vivo fluorescence without
692 oxygen, Nat. Biotechnol., **25**, 443-445 (2007).
693 61. **Drepper, T., Huber, R., Heck, A., Circolone, F., Hillmer, A. K., Büchs, J., and Jaeger, K. E.:**
694 Flavin mononucleotide-based fluorescent reporter proteins outperform green fluorescent

protein-like proteins as quantitative in vivo real-time reporters, Appl. Environ. Microbiol., **76**, 5990-5994 (2010).

62. **Kunze, M., Roth, S., Gartz, E., and Büchs, J.:** Pitfalls in optical on-line monitoring for high-throughput screening of microbial systems, Microb. Cell Fact., **13**, 53 (2014).

63. **Ude, C., Ben-Dov, N., Jochums, A., Li, Z. P., Segal, E., Scheper, T., and Beutel, S.:** Online analysis of protein inclusion bodies produced in *E. coli* by monitoring alterations in scattered and reflected light, Appl. Microbiol. Biotechnol., **100**, 4147-4159 (2016).

64. **Zhang, J. Y., Reddy, J., Buckland, B., and Greasham, R.:** Toward consistent and productive complex media for industrial fermentations: Studies on yeast extract for a recombinant yeast fermentation process, Biotechnol. Bioeng., **82**, 640-652 (2003).

65. **Tachibana, S., Watanabe, K., and Konishi, M.:** Estimating effects of yeast extract compositions on Escherichia coli growth by a metabolomics approach, J Biosci Bioeng, **128**, 468-474 (2019).

66. **Chalmers, J. J., Kim, E., Telford, J. N., Wong, E. Y., Tacon, W. C., Shuler, M. L., and Wilson, D. B.:** Effects of the temperature on *Escherichia coli* overproducing beat-lactamase or human epidermal growth-factor, Appl. Environ. Microbiol., **56**, 104-111 (1990).

67. **Vasina, J. A. and Baneyx, F.:** Expression of aggregation-prone recombinant proteins at low temperatures: A comparative study of the *Escherichia coli* cspA and tac promoter systems, Protein Expr. Purif., **9**, 211-218 (1997).

68. **Arie, J. P., Miot, M., Sassoon, N., and Betton, J. M.:** Formation of active inclusion bodies in the periplasm of *Escherichia coli*, Mol. Microbiol., **62**, 427-437 (2006).

69. **Korovashkina, A. S., Rymko, A. N., Kvach, S. V., and Zinchenko, A. I.:** Enzymatic synthesis of c-di-GMP using inclusion bodies of *Thermotoga maritima* full-length diguanylate cyclase, J. Biotechnol., **164**, 276-280 (2013).

70. **Morell, M., Bravo, R., Espargaro, A., Sisquella, X., Aviles, F. X., Fernandez-Busquets, X., and Ventura, S.:** Inclusion bodies: specificity in their aggregation process and amyloid-like structure, Biochim. Biophys. Acta, **1783**, 1815-1825 (2008).

71. **Jong, W. S., Vikstrom, D., Houben, D., van den Berg van Saparoea, H. B., de Gier, J. W., and Luirink, J.:** Application of an *E. coli* signal sequence as a versatile inclusion body tag, Microb. Cell Fact., **16**, 50 (2017).

72. **Kunze, M., Lattermann, C., Diederichs, S., Kroutil, W., and Büchs, J.:** Minireactor-based high-throughput temperature profiling for the optimization of microbial and enzymatic processes, J. Biol. Eng., **8**, 22 (2014).

73. **Mühlmann, M., Forsten, E., Noack, S., and Büchs, J.:** Optimizing recombinant protein expression via automated induction profiling in microtiter plates at different temperatures, Microb. Cell Fact., **16**, 220 (2017).

74. **Margreiter, G., Messner, P., Caldwell, K. D., and Bayer, K.:** Size characterization of inclusion bodies by sedimentation field-flow fractionation, J Biotechnol, **138**, 67-73 (2008).

75. **Bettenbrock, K., Fischer, S., Kremling, A., Jahreis, K., Sauter, T., and Gilles, E. D.:** A quantitative approach to catabolite repression in *Escherichia coli*, J Biol Chem, **281**, 2578-2584 (2006).

Captions

FIG. 1. Illustration of the fusion proteins and the resulting protein distribution within *E. coli* BL21(DE3). (A) Schematic illustration of the fusion of the coiled-coil domain (TDoT, domain of the cell surface protein tetrabrachion of *Staphylothermus marinus*, PDB-ID: 1FE6) to a linker peptide consisting of a $(GGGS)_3$ motif and a cleavage site for the protease factor Xa and the target protein YFP (monomeric yellow fluorescent protein of *Aequorea victoria*, PDB-ID: 1YFP). (B) Microscopic image of *E. coli* BL21(DE3) cells expressing TDoT-L-YFP show formation of fluorescent inclusion bodies. (C) Schematic illustration of the reference construct consisting of the linker peptide and the target protein (YFP). (D) Microscopic image of *E. coli* BL21(DE3) expressing L-YFP with fluorescence equally distributed within cells.

FIG. 2. Detailed characterization of the cultivation in complex TB autoinduction medium. Cultivation of *E. coli* BL21(DE3) TDoT-L-YFP (A-E) and L-YFP (F-J). (A+F) Oxygen transfer rate and temperature over time for *E. coli* BL21(DE3) expressing TDoT-L-YFP (insoluble) and L-YFP (soluble), respectively. For OTR, duplicates are displayed. Due to strong impact of the temperature shift on the oxygen sensor for OTR measurements, no OTR values are given in that period (dotted lines). (B+G) Scattered light intensity and offline OD_{600} as function of cultivation time. (C+H) Online YFP fluorescence and offline YFP fluorescence intensity of crude cell extract, soluble and washed insoluble fraction after cell disruption. For online fluorescence and scattered light, a median filter is applied and the mean of six wells with standard deviation is displayed. (D+I) Glucose, lactose, glycerol and acetate concentrations and pH. (E+J) SDS-PAGE analysis showing protein distribution per sample volume of soluble (S) and washed insoluble (I) fractions at 3, 10, 19, 29, 43, 56 and 72 h of cultivation. Arrows indicates size of target proteins (M = protein marker). Cultivation conditions (A+F): 250 mL RAMOS flask with 25 mL filling volume, 90 rpm shaking frequency, 50 mm shaking diameter. (B-E, G-J): 48-deepwell MTP with 2 mL filling volume, 600 rpm shaking frequency, 3 mm shaking diameter.

FIG. 3. Detailed characterization of the cultivation in minimal Wilms-MOPS autoinduction medium. Cultivation of *E. coli* BL21(DE3) TDoT-L-YFP (insoluble) (A-D) and L-YFP (soluble) (E-H). (A+E) Scattered light intensity and cultivation temperature as function of cultivation time for *E. coli* BL21(DE3) expressing TDoT-L-YFP (insoluble) and L-YFP (soluble). (B+F) Online YFP fluorescence and offline YFP fluorescence intensity of crude cell extract, soluble and washed insoluble fraction after cell disruption. (C+G) Glucose, lactose, glycerol and acetate concentrations and pH. (D+H) SDS-PAGE analysis showing protein content per sample volume of soluble (S) and washed insoluble (I) fractions at 3, 10, 21.5, 27, 32.5, 45.5 and 60 h of cultivation. Arrows indicates size of target proteins (M = protein marker). Cultivation conditions: 48-deepwell MTP with 2 mL filling volume, 600 rpm shaking frequency, 3 mm shaking diameter.

FIG. 4. Production of FIBs at a constant cultivation temperature of 37 °C. Cultivation of *E. coli* BL21(DE3) TDoT-L-YFP (A+B) and L-YFP (C+D) in Wilms-MOPS autoinduction medium (0.5 g/L glucose, 2 g/L lactose, 5 g/L glycerol). (A+C) Oxygen transfer rate as function of cultivation time. (B+D) Online YFP

779 fluorescence. (B insert) SDS-PAGE analysis showing protein content per sample volume of soluble (S) and
780 washed insoluble (I) fractions at the end of cultivation. Boxes indicate target protein (M = protein marker).
781 Duplicates are displayed in dashed lines and open symbols. For clearer graphical representation, symbols
782 are only displayed for every 3rd (A+C) and every 8th (B+D) data point, respectively. Cultivation conditions:
783 48-deepwell MTP with 2–0.4 mL filling volume, 600 rpm shaking frequency, 3 mm shaking diameter, 37
784 °C cultivation temperature.
785
786 FIG. 5. Production of FIBs at increasing maximum oxygen transfer capacities. Cultivation of *E. coli*
787 BL21(DE3) TDoT-L-YFP (A-C) in minimal Wilms-MOPS auto-induction medium (0.5 g/L glucose, 2 g/L
788 lactose, 5 g/L glycerol) at different maximum oxygen transfer capacities, achieved by varying the filling
789 volume (2.0 mL, 1.6 mL, 1.2 mL, 0.6 mL). (A) Scattered light intensity and cultivation temperature as
790 function of cultivation time. (B) Online YFP fluorescence. (C) Final fluorescence intensity of crude cell
791 extract, soluble and washed insoluble fraction at the end of cultivation. For clearer graphical representation,
792 symbols are only displayed for every 8th (A) and every 5th (B) data point, respectively. Cultivation
793 conditions: 48-deepwell MTP with 2–0.6 mL filling volume, 600 rpm shaking frequency, 3 mm shaking
794 diameter.
795
796 FIG. 6. Impact of autoinduction and different IPTG concentrations on FIB production. Cultivation of *E.*
797 *coli* BL21(DE3) TDoT-L-YFP in minimal Wilms-MOPS medium. Cultures induced with IPTG were
798 supplemented with 7.5 g/L glucose. IPTG (0 – 1 mM) was added after 4.5 h of cultivation (Arrow indicates
799 time of IPTG addition.). Cultures with autoinduction medium contained the standard carbon concentrations
800 (0.5 g/L glucose, 2 g/L lactose, 5 g/L glycerol). (A) Scattered light intensity and cultivation temperature as
801 function of cultivation time. (B) Online YFP fluorescence. (C) Final YFP fluorescence intensity of crude
802 cell extract and washed insoluble fraction after 46 h. Cultivation conditions: 48-deepwell MTP with 0.8 mL
803 filling volume, 1000 rpm shaking frequency, 3 mm shaking diameter. Duplicates for all cultivation
804 conditions are displayed.
805
806 FIG. 7. Production of FIBs in 2 L stirred tank reactor batch fermentation. *E. coli* BL21(DE3) TDoT-L-YFP
807 in minimal Wilms-MOPS autoinduction medium. Initial carbon source concentrations were 4.9 g/L

glucose, 19.7 g/L lactose and 49.2 g/L glycerol. (A) Oxygen transfer rate and cultivation temperature as function of cultivation time. (B) Optical density and cell dry weight. For cell dry weight, the mean of duplicates is displayed (C) Offline YFP fluorescence of crude cell extract, soluble and washed insoluble fraction. (D) Glycerol, lactose and glucose concentration. (E) Final cell dry weight (mean of duplicates), FIB concentration (mean and standard deviation of triplicates displayed), yield coefficient of FIB concentration per cell dry weight ($Y_{FIB/CDW}$), yield coefficient of FIB concentration per initial carbon source concentrations ($Y_{FIB/S}$) and space time yield (STY; FIB production per liter and hour). Cultivation conditions: 1.5 L working volume, 0.5 vvm aeration rate, DOT controlled at 30 % air saturation by adjusting the stirring rate, pH controlled at 7 using 25% (w/v) ammonia solution.

818 **Figures**

819

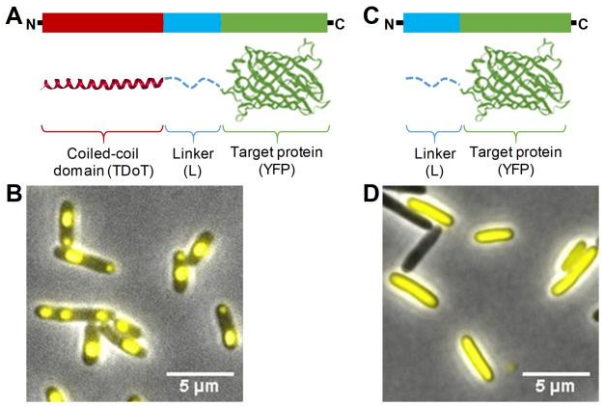

820

821 FIG. 1.

822

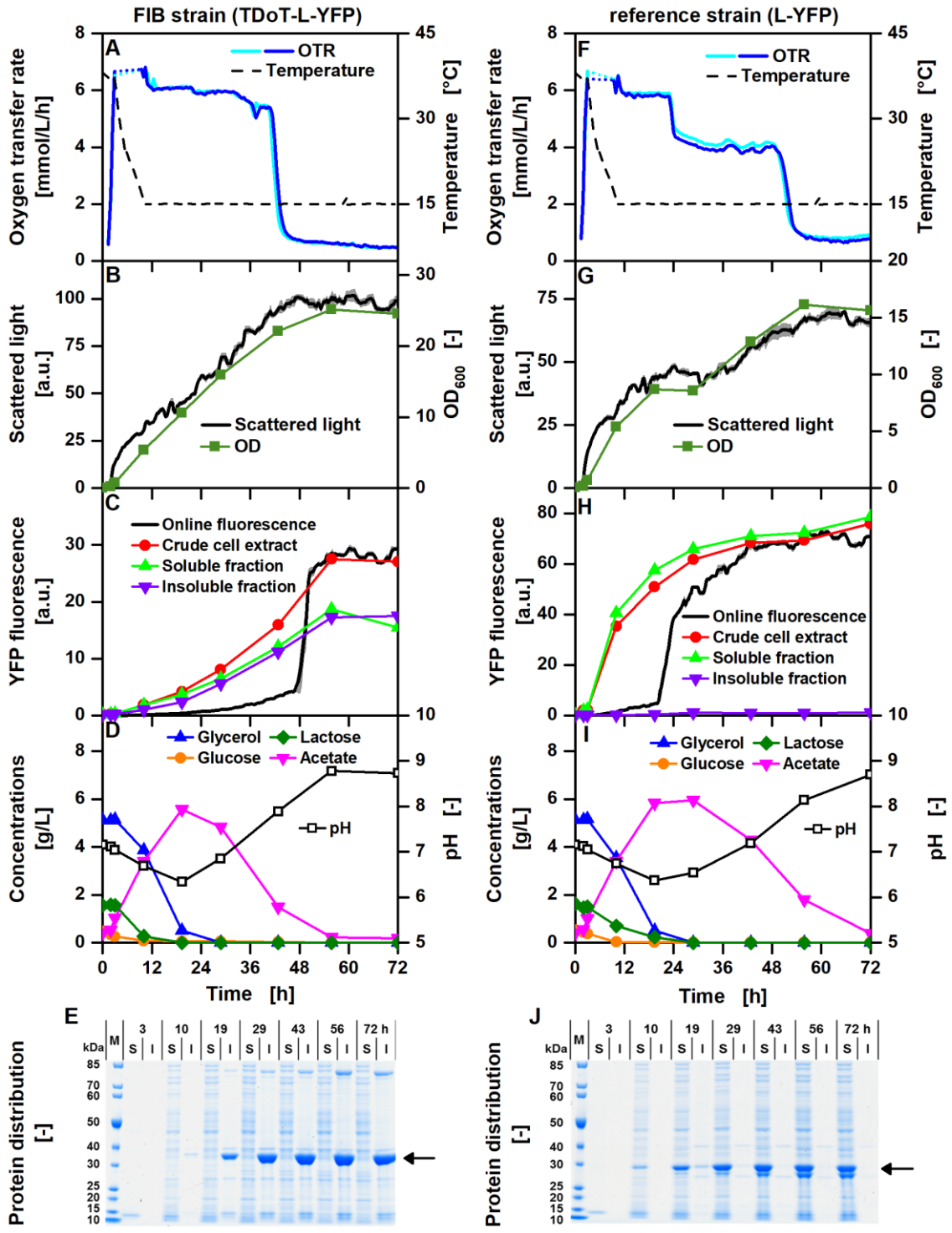
FIB strain (TDoT-L-YFP)
reference strain (L-YFP)
A
F
OTR
Temperature
Oxygen transfer rate [mmol/L/h]
Temperature [°C]
B
G
Scattered light
OD
Scattered light [a.u.]
OD600 [-]
C
H
Online fluorescence
Crude cell extract
Soluble fraction
Insoluble fraction
YFP fluorescence [a.u.]
D
I
Glycerol
Lactose
Glucose
Acetate
pH
Concentrations [g/L]
pH [-]
Time [h]
E
J
kDa
M
3
10
19
29
43
56
72 h
S
I
Protein distribution [-]

FIG. 2.

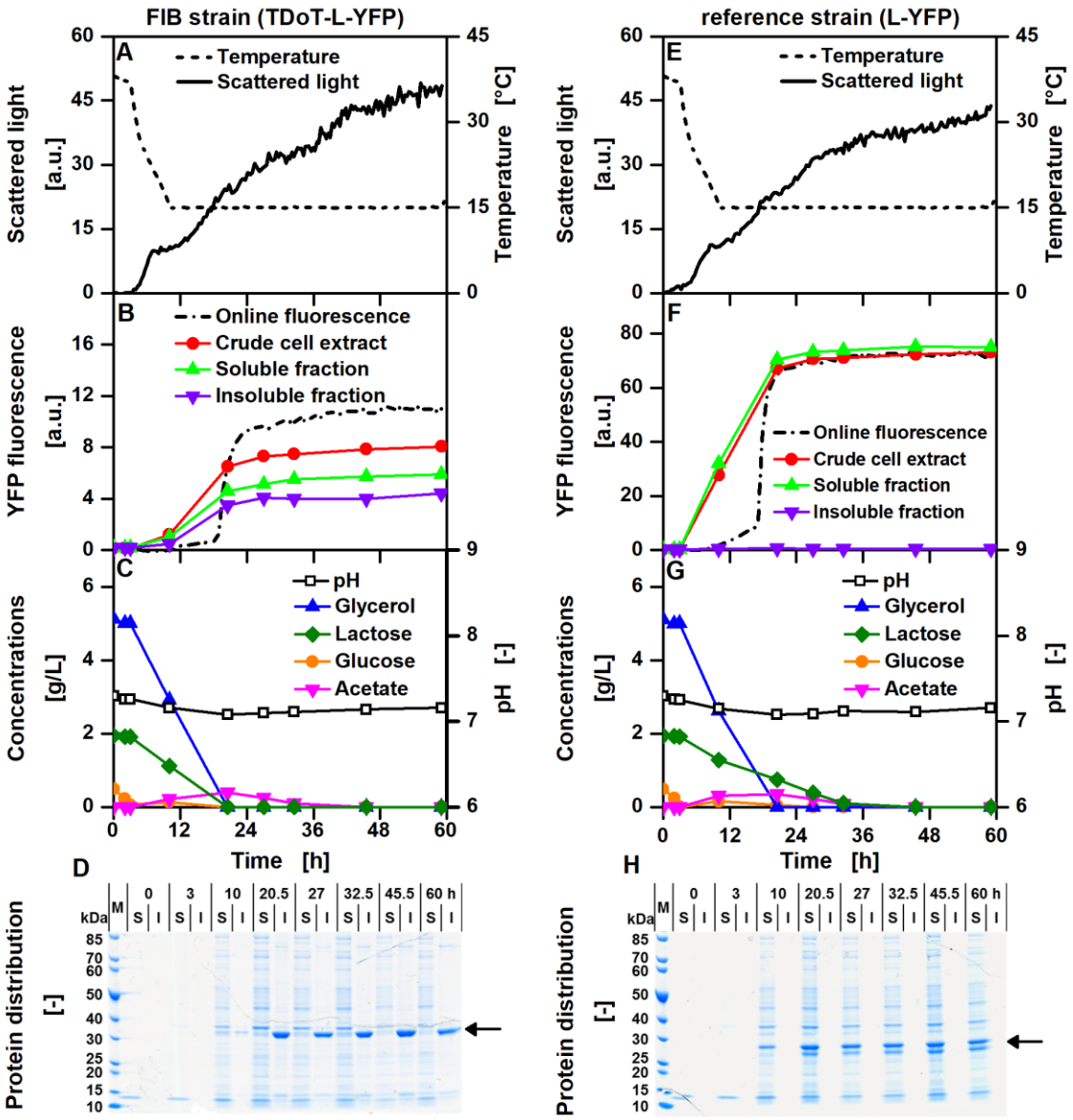
FIB strain (TDoT-L-YFP)
reference strain (L-YFP)
A
E
Temperature
Scattered light
Scattered light [a.u.]
Temperature [°C]
B
F
Online fluorescence
Crude cell extract
Soluble fraction
Insoluble fraction
YFP fluorescence [a.u.]
C
G
pH
Glycerol
Lactose
Glucose
Acetate
Concentrations [g/L]
pH [-]
Time [h]
D
H
kDa
M
0
3
10
20.5
27
32.5
45.5
60 h
S
I
Protein distribution [-]

FIG. 3.

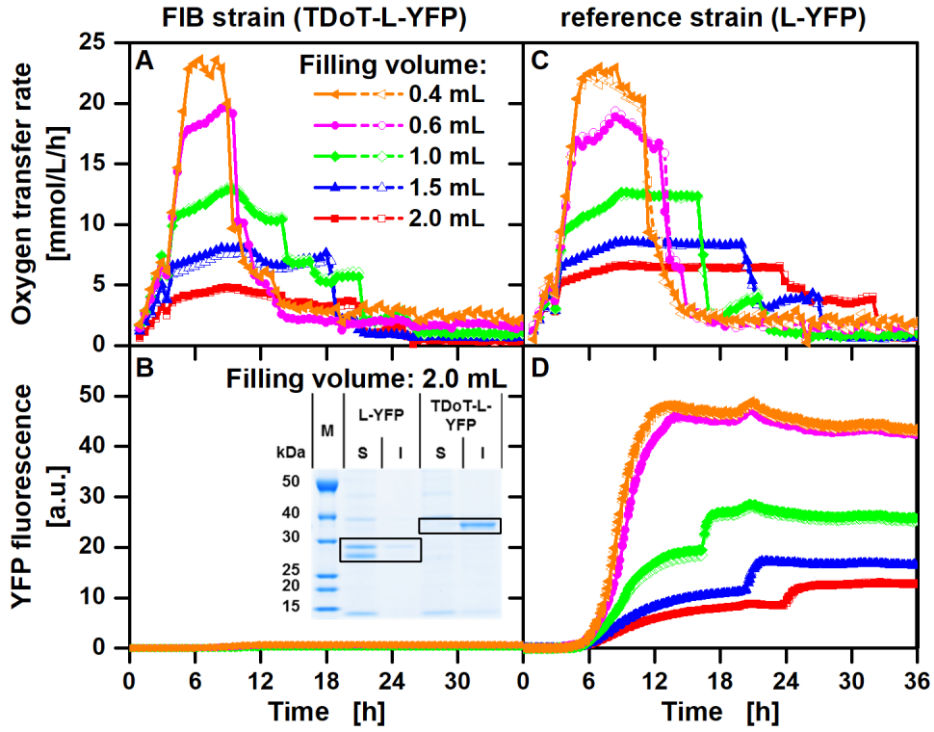
FIB strain (TDoT-L-YFP)
reference strain (L-YFP)
A
B
C
D
Filling volume:
0.4 mL
0.6 mL
1.0 mL
1.5 mL
2.0 mL
Filling volume: 2.0 mL
Oxygen transfer rate [mmol/L/h]
YFP fluorescence [a.u.]
Time [h]
Time [h]
M
L-YFP
TDoT-L-YFP
kDa
S
I
S
I
50
40
30
25
20
15

FIG. 4.

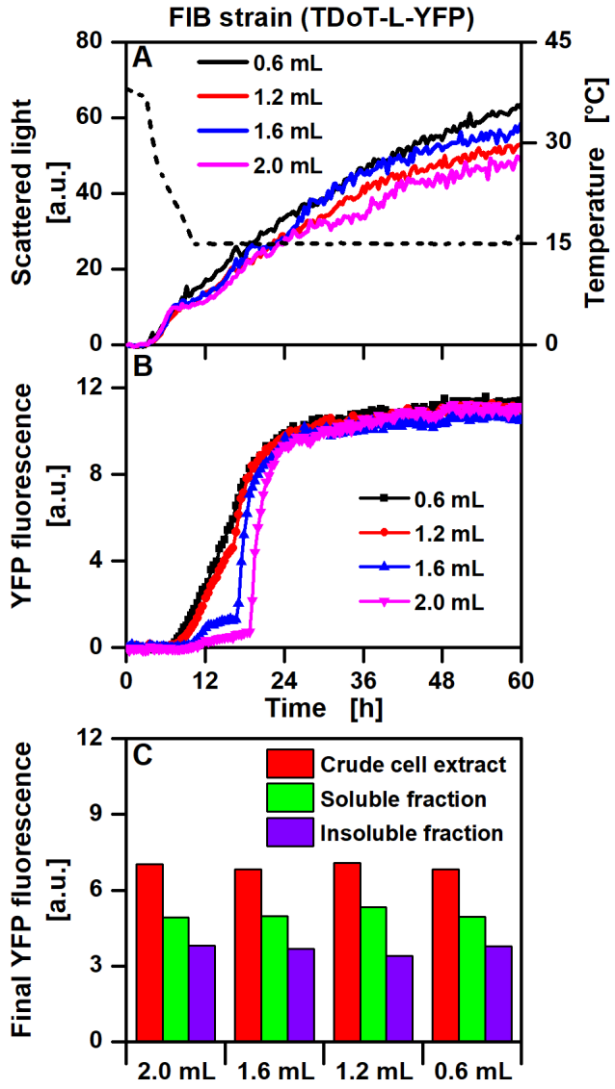
FIB strain (TDoT-L-YFP)
A
0.6 mL
1.2 mL
1.6 mL
2.0 mL
Scattered light [a.u.]
Temperature [°C]
B
YFP fluorescence [a.u.]
Time [h]
C
Crude cell extract
Soluble fraction
Insoluble fraction
Final YFP fluorescence [a.u.]
2.0 mL
1.6 mL
1.2 mL
0.6 mL

FIG. 5.

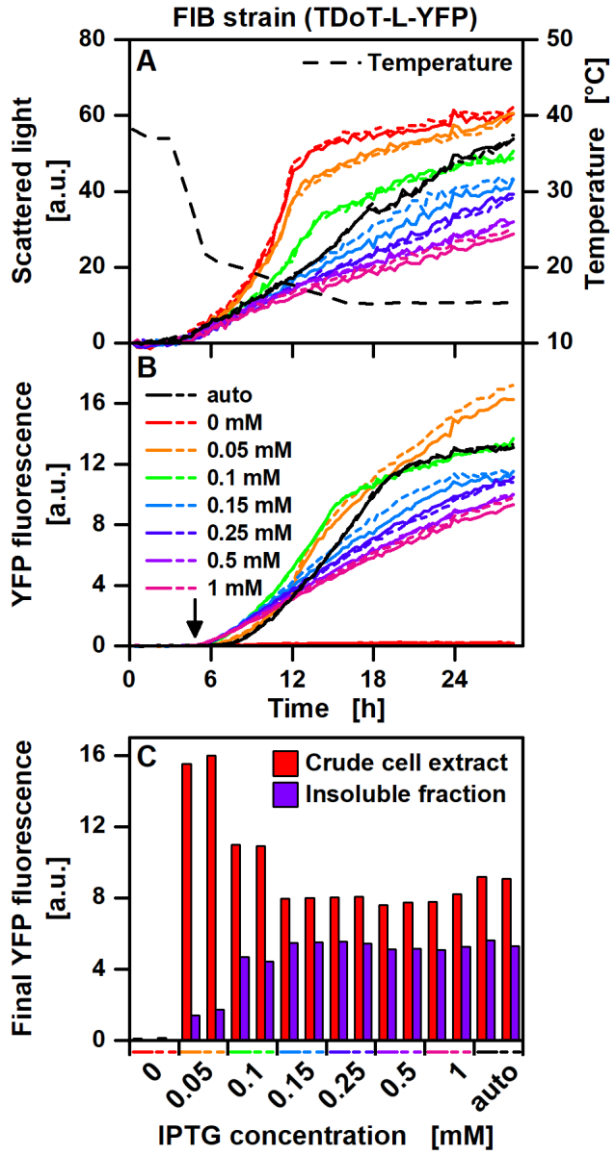
FIB strain (TDoT-L-YFP)
A
Temperature
Scattered light [a.u.]
Temperature [°C]
B
auto
0 mM
0.05 mM
0.1 mM
0.15 mM
0.25 mM
0.5 mM
1 mM
YFP fluorescence [a.u.]
Time [h]
C
Crude cell extract
Insoluble fraction
Final YFP fluorescence [a.u.]
IPTG concentration [mM]

FIG. 6.

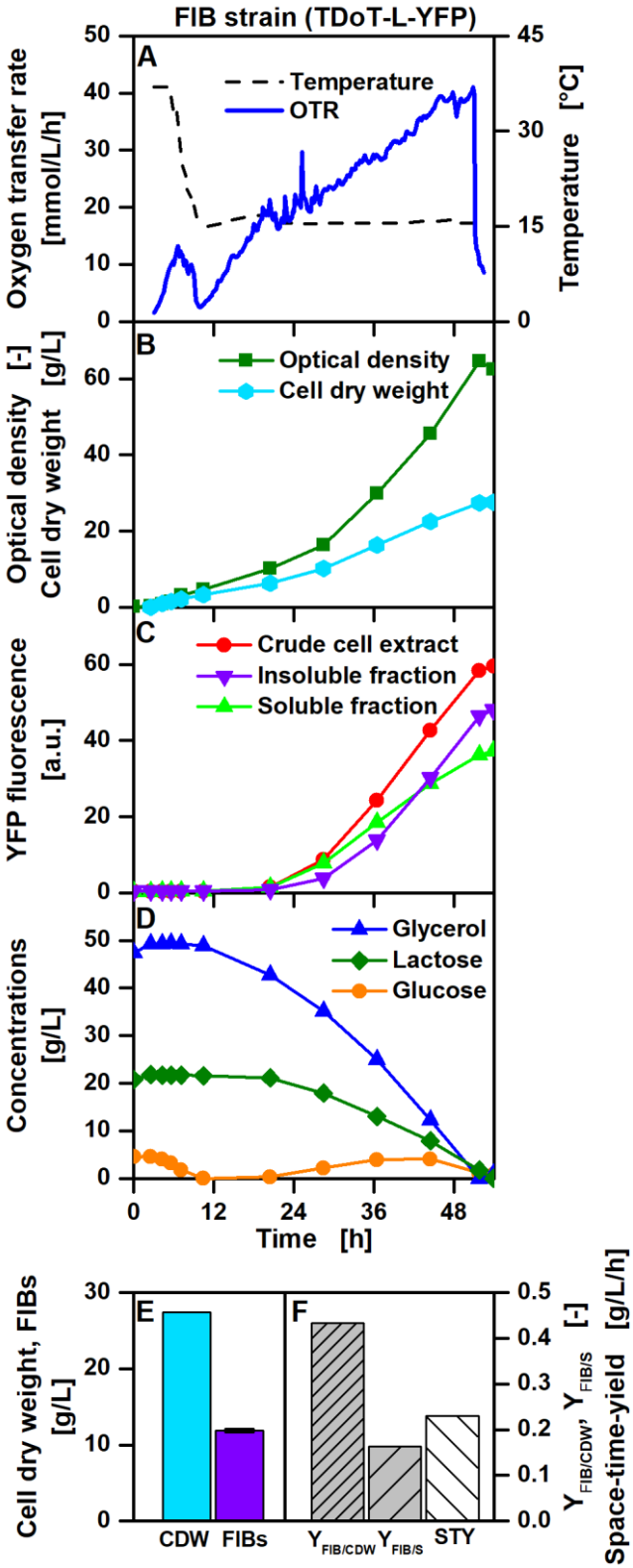

841

842 FIG. 7.

843
844